SLAC Proposal E-154 October 1, 1993

A PROPOSAL FOR A PRECISION MEASUREMENT OF THE NEUTRON SPIN STRUCTURE FUNCTION USING A POLARIZED HELIUM-3 TARGET

R.G. Arnold, P.E. Bosted, S.E. Rock, J.L. White, Z.M. Szalata

American University, Washington, DC 20016

V. Breton, H. Fonvieille, Y. Roblin

LPC IN2P3/CNRS, Université Blaise Pascal, F-63170 Aubière, Cedex, France

R. Fuzesy, D. Pripstein, G. Shapiro

University of California and LBL, Berkeley, CA 94720

H. Borel, R.M. Lombard-Nelsen, J. Marroncle, F. Staley, Y. Terrien

Centre d'Etudes de Saclay, DAPNIA/SPhN, F-91191 Gif-sur-Yvette, France

B.D. Anderson, R. Madey, D.M. Manley, G.G. Petratos*, J.W. Watson

Kent State University, Kent, OH 44242

F.S. Dietrich

Lawrence Livermore Laboratory, Livermore, CA 94550

T.E. Chupp, K. Coulter, T. Smith

University of Michigan, Ann Arbor, MI 48109

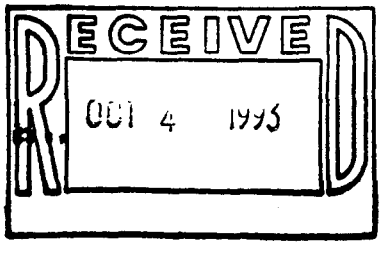

A.K. Thompson

National Institute of Standards and Technology, Gaithersburg, MD 20899

S. E. Kuhn

Old Dominion University, Norfolk, Virginia 23529

G.D. Cates, K. Kumar, H. Middleton

Princeton University, Princeton, NJ 08544

P.L. Anthony, H. Dutz[†], R. Gearhart,

E.W. Hughes, D. Kawall, T. Maruyama, W. Meyer[†], R. Pitthan,

S.H. Rokni, L.M. Stuart, M. Woods, C.C. Young

Stanford Linear Accelerator Center, Stanford, CA 94309

R. Holmes, P.A. Souder, J. Xu

Syracuse University, Syracuse, NY 13210

L. Auerbach, J. Margulies, J. Martoff, Z.-E. Meziani

Temple University, Philadelphia, PA 19122

H.R. Band, J.R. Johnson, R. Prepost, G. Zapalac

University of Wisconsin, Madison, WI 53706

Spokesperson: Emlyn Hughes (415) 926-4794

---

* present address: MS 20, SLAC, Stanford, CA 94309

† permanent address: Universität Bonn, Nußallee 12, 53115 Bonn 1, Germany

ABSTRACT

We propose to measure the neutron spin structure function g_1^n over x ranging from 0.015 to 0.7 and Q^2 ranging from 1 to 16 GeV^2. This measurement uses a 48.6 GeV polarized electron beam scattering off a polarized ^{3}He target. Such a measurement will address the considerable theoretical interest in the neutron spin structure and allow for a precision test of the Bjorken sum rule at a high average Q^2 ($Q^2 \sim 5$ GeV^2). We expect this measurement will determine the integral over the neutron spin structure function to a precision of $\pm$ 0.003 (stat.) and $\pm$ 0.004 (syst.), approximately a factor of two more precise than experiment E-142. In addition, this measurement will be at more than double the average Q^2 of experiment E-142. The higher Q^2 and higher precision measurement allows for a more reliable extraction of the quark parton model parameters, Δs and Δq.

1. Introduction and History

In 1988 the EMC collaboration at CERN revived an interest in an old field of physics by reporting on proton spin structure function measurements at low x using high energy muon scattering [1]. The EMC results violated a QCD sum rule of Ellis and Jaffe [2] and these results were interpreted to mean that the quarks carried little of the proton spin, and the strange sea was highly polarized ($\sim$ 20%). Hundreds of theoretical papers followed, and three experimental programs were proposed at CERN (SMC) [3], DESY (HERMES) [4], and SLAC (E-142 and E-143). In addition, numerous low energy polarized electron and neutrino scattering experiments have been proposed to examine specifically the strange sea polarization [5].

In 1993 two experiments reported on first measurements of the neutron spin structure function, g_1^n, concurrently at the QCD Moriond Conference. The SMC experiment extracted the neutron spin structure function using a polarized deuterium target and found the neutron integral over x to be $\int_0^1 g_1^n(x)dx = -0.08 \pm 0.04 \pm 0.04$ [6]. The E-142 collaboration [7] (Appendix B) reported a result of $\int_0^1 g_1^n(x)dx = -0.022 \pm 0.007 \pm 0.009$ in which the measured range of x was $0.03 < x < 0.6$ and the contribution to g_1^n outside the measured range came from extrapolations, following a Regge behavior at low x and a quark parton model (QPM) inspired model at high x.

From the spin structure function measurements of EMC g_1^p and SLAC E-142 g_1^n one gets

$$\int_0^1 g_1^p(x)dx - \int_0^1 g_1^n(x)dx = 0.146 \pm 0.022$$

and from the Bjorken sum rule evaluated only up to first order in α_s, the prediction is:

$$\int_0^1 g_1^p(x)dx - \int_0^1 g_1^n(x)dx = 0.187 \pm 0.004,$$

where the uncertainty in the integral comes from the uncertainty in α_s at the different Q^2 of the two experiments.

At first glance, a two standard deviation difference appears between the SLAC result and the Bjorken sum rule. However, higher order perturbative (α_s^2, α_s^3 terms) [8] and non-perturbative [9] QCD corrections (known as "higher twist corrections") indicate that this apparent discrepancy vanishes [10]. Figure 1 shows a comparison of the measured proton minus neutron integral to the theoretical prediction including just the perturbative QCD corrections.

Since the higher order PQCD corrections are large (and have large uncertainties) at low Q^2 (as in E-142), the goal is to measure these integrals with high precision at higher Q^2. In response to this situation, this document proposes to remeasure the neutron spin structure function as extracted from ^{3}He using a 48.6 GeV polarized electron beam. The precision to which the neutron integral is determined will approximately match statistical (± 0.003) and estimated systematic (± 0.004) uncertainties. At this energy, the average Q^2 of the neutron integral will be ~ 5 GeV^2, compared to 2 GeV^2 from experiment E-142.

The second important motivation for measuring the neutron spin structure function to as high a precision as possible is to test the Quark Parton Model (QPM). The two questions to be answered are (1) do the quarks carry the spin of the nucleon and (2) is the strange sea in the nucleon highly polarized? To answer

these questions requires only a single measurement of either the proton or neutron integral. Appendix A gives a description of how one extracts the total quark and strange quark contribution to the nucleon spin in the QPM. It should be stressed that the second motivation argues to determine the neutron integral as accurately as possible independent of the proton integral uncertainty which will have a **larger** systematic uncertainty. The larger systematic uncertainty on the proton integral arises from the fact that the proton asymmetries are large and many systematic uncertainties (i.e. target and beam polarizations, dilution factor) scale with the size of the asymmetry.

We submit that our proposed experiment at 50 GeV will greatly help to resolve the difficult theoretical issues involving the nucleon structure functions. The higher Q^2 of the present proposal makes the interpretation in terms of the QPM more reliable than for E-142.

For a successful experiment four projects have to come together: (1) a highly polarized beam of 48.6 GeV, (2) a beam polarimeter of good precision, (3) a polarized ^{3}He target of sufficient polarization, and (4) a spectrometer package which can handle the short beam pulse (120 nsec) of the SLED'ed beam and the higher π/e ratio at higher energy.

As a collaboration we have little possibility to impact on the performance of (1), we believe we have (2) and (3) well under control, so most of our effort for the experiment will go into (4). The conceptual spectrometer design, therefore, takes most of the space in the following discussion.

2. Polarized Beam

New developments of high polarization electron sources at SLAC have attained polarizations on the order of $\sim$ 80%. The experiment will benefit greatly from the higher beam polarization (versus 40% in E-142), which essentially compensates for the loss in events from the smaller scattering cross section at higher energy ($d\sigma \sim 1/E^2$). E-142 ran with on average a 23 GeV beam. The assumed beam conditions for this proposal are given in Table 1.

As has been pointed out [12] the 50 GeV beam will suffer emittance growth during the transport from the LINAC to End Station A due to synchrotron radiation in an area of considerable dispersion. The larger beam spot ($\sim$ 2 mm) does not impact on this experiment, as long as the beam halo intensity at the location of the walls of the glass target cell is no more than 10^{-5} of the central intensity. Since the glass wall is at 5 σ of the beam diameter at the target, and since the emittance growth is based on a statistical process, we do not foresee any problem.

Table 1.

Beam conditions	
Polarization	80 %
Intensity	10^{11} e^- / pulse
Pulse Length	120 nsec
Beam Halo	10^{-5} at 10 mm

3. Polarized ^{3}He Target

The physics of the polarized ^{3}He target is well established [11], and the successful E-142 target has been documented [13]. The ^{3}He is contained in a two-chambered aluminosilicate glass cell. The "pumping chamber", which also contains several milligrams of rubidium metal, is heated to achieve a dense vapor of Rb. The "target chamber", through which the electron beam passes, is connected to the pumping chamber by a transfer tube. The Rb is optically pumped using 795 nm light from titanium sapphire lasers, and subsequently polarizes the ^{3}He nuclei by spin exchange collisions. The time constants characterizing Rb–^{3}He *spin exchange* are extremely long, on the order of many hours. To achieve high polarizations, it is thus critical that the time constants characterizing *spin relaxation* are even longer, on the order of many tens of hours. All the cell building techniques developed for E-142 will be utilized, and should be quite adequate for the experiment.

Based on our experience in E-142, we are planning several small improvements to the ^{3}He target:

1. The oven with which the "pumping cell" is heated will be constructed from a higher temperature plastic than was previously used. This will make it possible to run at higher temperatures, thus enhancing spin exchange and making it possible to make better use of our laser light.
2. The windows will be thinner. This will be made possible by utilizing a concave window design that has better pressure resistance.
3. The laser cave can accommodate six lasers, while only five were used for E-142. A sixth laser will be used.

Improvements (1) and (3) will result in higher polarization, and improvement (2) will improve our dilution factor. While it may be possible to reach an even thinner glass window with the concave design, we have not built such a window at the present time.

The ^{3}He target parameters are given in Table 2.

Table 2.

^{3}He target parameters		
Parameter	E-142	E-154
Density	9 atms	10 atms
Window thickness	0.12 mm	0.10 mm
Polarization	35 %	40 %

A new scattering chamber which matches the target vacuum chamber and the spectrometer magnets will have to be built. Finally, some modifications to the optical beam path are planned to increase efficiency in maintaining target polarization running with the target polarized in the transverse direction. During the E-142 experiment, the polarization of the target decayed when collecting data for determining A_2. For this experiment we plan to maintain a steady transverse target polarization by changing the optical beam path to illuminate the ^{3}He cell in the direction transverse to the electron beam.

4. Spectrometer Systems

General Design Concepts

The philosophy of the spectrometer systems (i.e., magnetic and detector elements together) for the 50 GeV spin structure physics program will be based on the E-142 design [14], described in detail in Appendix C. The design has proven to work adequately for the needs of E-142.

Each spectrometer will use the S-bend configuration of E-142 (two dipole magnetic elements with opposite deflection) that maximizes the available solid angle and at the same time suppresses neutral particle background originating from the target.

The detector packages must attempt to closely match the magnetic design, and visa versa, and the requirements of spin structure function physics. Following the E-142 example [14], the conceptual design presented here attempts to optimize the transverse area which has to be filled with detector elements to the requirements of the specific spin physics of E-154 and E-155, and thus to minimize cost.

In a joint meeting in early September the E-154 and E-155 collaborations reached an agreement on the two spectrometer angles, foreseen to be at 2.75° and 5.5°. These angles are the optimal compromise between the desire for low x and high momentum transfer.

A joint "spectrometer working group" of E-154 and E-155 will decide between different, but not too dissimilar, S-bend options that will satisfy the needs of both experiments. These configurations include a possible further evolution of the E-142 design towards a novel S-bend configuration in the vertical combined with a horizontal third dipole element to bend the scattered electrons away from the

beam pipe [15]. Such a design could be particularly appropriate for the smaller angle spectrometer where, due to the proximity to the straight ahead beam pipe, shielding could be a problem. Therefore, what is described here (and, by the same token, in the E-155 proposal) is a lay-out of principles which need to be heeded, rather than a definite design.

Magnetic Elements

The essential magnetic elements of the spectrometers using a cost-effective design along the lines of E-142 are (see Figure 2):

- A large angle spectrometer using only two dipoles.
- A small angle spectrometer using two dipoles, possibly augmented by an additional quadrupole.

Cost effective for the magnetic elements means a design which needs neither new water nor new electrical utilities, and a minimum of new magnetic measurements. The principal difference to E-142 will be the replacement of the upstream dipole in the large angle spectrometer with the front-notched C-type dipole from the 20 GeV/c spectrometer.

The solid angles and momentum resolutions will be very similar to the large and small angle E-142 spectrometers. The pattern of the E-142 spectrometer deflection angles, where the upstream dipole bends less than the downstream one, making the system non-achromatic, will be preserved. This will allow for sufficient momentum resolution without having to introduce additional quadrupoles.

The range of relative momentum acceptance will be from $\sim -50\%$ to $\sim +100\%$. A choice of 20 GeV/c of central momentum will cover the required momentum range of $\sim$10 to $\sim$40 GeV/c for the 48.6 GeV expected beam energy.

The optics of the 5.5° spectrometer will be similar to the non-focusing optics of the 7° E-142 spectrometer. Experience from E-142 indicates that the rates in the existing hodoscopes, projected to 50 GeV, will be low enough in this spectrometer to allow for momentum and scattering angle determination through tracking.

The optics of the 2.75° spectrometer, where the rates are higher, could be variably focusing by tuning the quadrupole. If needed, the quadrupole can provide a momentum focus for low energy particles as in the E-142 design. Preliminary calculations indicate that non-focusing optics, but with improved, finer, hodoscope segmentation, could be possible. The true advantage of using the quadrupole between, rather than behind the two dipoles, is that in either case (quadrupole on or off) the required sizes of the downstream detector elements are not dramatically different, and more space is provided for longer Čerenkov counters needed for improved π rejection at the higher energy (see below). More detailed calculations are needed to converge on a definite design.

The use of collimators in front of the upstream dipoles for both spectrometers in conjunction with proper spatial orientation of the dipoles themselves **will not allow photons originating from the target to reach the hodoscopes.** In the E-142 design [14] the latter could still happen after two bounces on the magnet apertures. With this new arrangement the background in the hodoscopes will be significantly reduced.

Detector Elements

The essential conceptual elements of the detector package are:

- Use of hodoscope tracking to measure the momentum and production angle

of scattered particles and to identify, understand and control backgrounds in the analysis.

- Use of two gas threshold Čerenkov counters in each spectrometer arm for pion rejection.
- Use of lead glass calorimetry for determining the scattered electron energy and production angle and for additional pion rejection.

A possible detector configuration, which uses heavily existing detector materials and electronics, matched to the magnet configuration, could be the following:

- Use of **two 6 m long** Čerenkov counters in each spectrometer **in tandem**, instead of the 2 and 4 m counters now in use. Since the E-142 Čerenkov tanks are modular in design this can easily be accomplished. At the same time, lowering the operating pressure to 1.5 psi will raise the π rejection threshold from 9 and 13 GeV for the short and long tank, respectively, to 19 GeV for both. This scheme will retain the high E-142 efficiency ($\sim$99%) with 5 photoelectrons per incident electron **per counter phototube.**
- Use of a **single** lead glass calorimeter of **uniform** characteristics in a fly's eye configuration in each spectrometer. Since the demands on segmentation are modest, use of the existing lead glass calorimeters seems possible and is under investigation. Their resolution seems to be sufficient for the highest **meaningful** x-bin (x$\sim$0.7) of statistical significance, which excludes events from nucleon resonance scattering.
- Use of the two **existing** 7° spectrometer hodoscopes in the new 5.5° spectrometer. Finer segmentation hodoscopes will be needed for any spectrometer design for the 2.75° spectrometer. The material of the existing small angle

spectrometer hodoscopes **will cover part** of the needed plastic scintillator and phototubes.

5. Run Plan

The bulk of this experiment will be concentrated at the highest energy to obtain a measurement at low x and the highest average Q^2. However, significant run time will be used to perform systematic studies. Measurements of the transverse spin asymmetries will be performed, optimized to reduce the error on the extraction of g_1^n and to obtain reasonable error bars on the neutron asymmetries A_1^n. A significant fraction of run time will also be used to study variations in beam conditions that might affect the dilution factor determination. These runs use a dummy target cell with variable pressure. For E-142, the dilution factor was our largest systematic error. Our view, in retrospect, is that having about twice as many dummy cell runs would reduce significantly the systematic uncertainty on the dilution factor determination. Finally, a subtraction of the electron background from charge symmetric hadronic decays will require about two days of beamtime.

Nine days of lower energy running at 30 GeV is planned in order to study radiative corrections and to provide a complete set of neutron spin structure function measurements as a function of x and Q^2. This data in combination with the E-142 20 GeV data and the E-154 50 GeV data will give a precise determination of the neutron spin structure function over a large range of x and Q^2. The 30 GeV data sample will be complementary to the proton and deuteron data set collected at 30 GeV in the E-143 experiment.

Assuming the run time of Table 3 and a 30% overall experimental efficiency (E-142 had a 30% efficiency), the statistical error on the neutron integral will be

Table 3.

Run plan	
Beam set up and check out	7 days
A_1 data	38 days
A_2 data	2 days
Dummy cell runs	3 days
Positron runs	2 days
30 GeV run	9 days

$\pm$ 0.003 over an x range from 0.015 to 0.7. The estimated systematic error on the neutron integral will be 0.004 as given in Table 1. This estimate depends on the value of the neutron integral, since most systematic errors scale with the answer. Projected results of the neutron asymmetry and structure function are given in Figures 3 and 4. It should be noted that only statistical error bars are shown, and that these are the dominant error on a point-to-point basis. Most systematic uncertainties scale with the size of the asymmetry, and the neutron asymmetries are small.

The results from this experiment will be at a much higher Q^2 than E-142 as shown in Figure 4. The large lever arm in studying Q^2 with a high precision is one of the true strengths of this SLAC program as compared to either HERMES (limited to 30 GeV) or CERN (limited statistical precision).

This Table assumes that the neutron integral value is -0.022 as measured in E-142. If the value changes, then some systematic uncertainties will scale up or down accordingly.

Table 4.

Systematic Uncertainties on the Neutron Integral		
Uncertainty	E-154	E-142
Beam polarization	0.001	0.001
Target polarization	0.001	0.002
Dilution factor	0.001	0.003
Uncertainty on F_2	0.001	0.002
Low x extrapolation	0.002	0.006
High x extrapolation	0.002	0.003
Radiative corrections	0.001	0.002
Positron subtraction	0.001	0.001
Pion subtraction	0.001	0.001
A_2^n	0.002	0.003
Total	0.004	0.009

6. Nuclear Effects

The determination of the inelastic spin-dependent structure function of the neutron from a measurement on ^{3}He relies on our understanding of the reaction mechanism of the virtual photon combined with the use of a realistic ^{3}He wave function. A detailed investigation of the ^{3}He inelastic spin response functions versus that of a free neutron has been carried out by three expert groups in few-body problems[17,18,19]. They examined the effect of the Fermi motion of nucleons and their binding in ^{3}He along with the study of the electromagnetic interaction treatment using the most realistic ^{3}He wave function. Consistent findings have been reached among the three groups, and we summarize here those relevant to our experiment:

- In the deep inelastic region an effective neutron spin structure response can be extracted from that of ^{3}He using a procedure in which S, S' and D states of the ^{3}He wave function are included, but no Fermi motion or binding effects are introduced:

$$\widetilde{g_1^n} = 1/P_n(g_1^{^3He} - 2P_p g_1^p)$$

where $\widetilde{g_1^n}$, g_1^p and $g_1^{^3He}$ are the spin structure functions of an effective free neutron, a free proton and ^{3}He, respectively. $P_n = (87 \pm 2)\%$ and $P_p = (-2.9 \pm 0.3)\%$ are the polarization values of the neutron and proton in ^{3}He due to the S, S$'$ and D states of the wave function [18]. *The Convolution approach calculations using the "exact" ^{3}He wave function including the full treatment of Fermi motion and binding effects show negligible differences with the above approximation.* A precise proton measurement is important to minimize the error on the correction. From the present experimental asymmetry data on the proton (SLAC E-80, E-130 and EMC) and that of the neutron (E-142) we can state that the uncertainty due to nuclear effects is negligible. At worst, it adds an **absolute uncertainty of $\Delta A_1^n \sim 2\%$** to the measured asymmetries.

- Contrary to the *deep inelastic region* the *quasielastic region* is much more sensitive to nuclear effects and has to be treated using the complete convolution method for a reliable extraction of the elastic neutron form factor. We point out that this is **of no concern** in this experiment since our proposed measurements have a lower limit in missing mass W^2 of 4 GeV^2, already well beyond the quasielastic and resonance region[19].

In addition, it is known that shadowing plays an important role in nuclei.

However, in the region of x and Q^2 covered by the proposed measurements for ^{3}He and deuteron nuclei, the anticipated effects are small. We believe that for this proposal with its quoted experimental uncertainty, nuclear effects and their corrections are still not yet of serious concern.

7. Summary

The goal of the present ^{3}He experiment is to build on the work begun in experiment E-142. A high precision neutron result at a high average Q^2 is necessary to compare to the high Q^2 proton result in order to test the Bjorken sum rule. And a high Q^2 measurement of the neutron spin structure function will also test the stability of the neutron result over a range of Q^2 needed to interpret the nucleon spin structure in the Quark Parton Model. At present, only the 50 GeV electron beam facility at SLAC could provide a result with such a lever arm.

REFERENCES

[1] J. Ashman *et al.*, Phys. Lett. **B206**, 364 (1988); Nucl. Phys. **B328**, 1 (1989).

[2] J. Ellis and R. Jaffe, Phys. Rev. **D9**, 1444 (1974).

[3] SMC proposal, V.W. Hughes *et al.* , CERN/SPSC 88-47 (1988).

[4] HERMES proposal, R. Milner and K. Rith *et al.* , DESY (1990).

[5] G. Garvey *et al.* , Preprint LA-UR-93-0037 (Dec. 1992).

[6] B. Adeva *et al.*, Phys. Lett. **B302**, 533 (1993).

[7] P.L. Anthony *et al.* , Phys. Rev. Lett. **71**, 959 (1993).

[8] S.A. Larin and J.A.M. Vermaseren, Phys. Lett. **B259**, 345 (1991).

[9] I.I. Balitsky *et al.* , Phys. Lett. **B242**, 245 (1990).

[10] J. Ellis and M. Karliner, CERN preprint, CERN-TH-6898/93 (1993).

[11] T.E. Chupp *et al.* , Phys. Rev. **C45**, 915 (1992); **36**, 2244 (1987).

[12] T. Fieguth, private communication.

[13] H. Middleton *et al.*, invited talk given at the 1993 Conference on Physics with Polarized Beams and Polarized Targets, Madison, WI.

[14] G.G. Petratos *et al.*, SLAC-PUB-5678 (1991); Proceedings of the IEEE Symposium of Nuclear Science, Santa Fe, NM (Nov. 1991).

[15] G.G. Petratos, presentation to the E-142/E-143 joint collaboration meeting, September 10, 1993.

[16] D. Kawall, *et al.*, Proceedings of the IEEE Symposium of Nuclear Science, Santa Fe, NM (Nov. 1991).

[17] B. Blankleider and R.M. Woloshyn, Phys. Rev. **C29**, 538 (1984).

[18] C. Ciofi degli Atti, S. Scopetta, E. Pace, G. Salme University of Perugia report N0. DFUPG-75/93, 1993.

[19] R.-W. Schulze and P.U. Sauer, Phys. Rev. **C48**, 38 (1993).

FIGURE CAPTIONS

Figure 1. Comparison of present day measurements of the Bjorken sum rule with the theoretical predictions including perturbative QCD corrections. Precision tests of this sum rule are only beginning to be accomplished at low Q^2.

Figure 2. The small (4.5°) and large (7.0°) angle E-142 spectrometer systems. A similar design is being considered for the small (2.75°) and large (5.5°) angle E-154 spectrometers. The principal difference in the new set-up would be the replacement of the upstream dipole (B202) in the large angle spectrometer by the C-type upstream dipole (B201) from the 20 GeV/c spectrometer.

Figure 3. Projected statistical error bars on the neutron asymmetries A_1^n from E-154 compared to those achieved by E-142. Note, however, that the E-154 results are at much larger Q^2, and much less susceptible to low Q^2 theoretical corrections, as depicted in Figure 1. Results for the calculations of the statistical error bars are given separately for the two spectrometer arms at 2.75° and 5.5°.

Figure 4. Projected statistical error bars on the neutron spin structure function measurement g_1^n as compared to those achieved in E-142. Results for the calculations of the statistical error bars are given separately for the two spectrometer arms at 2.75° and 5.5°.

Figure 5. Projected x and Q^2 ranges accessible to E-154 at 49 GeV versus E-142.

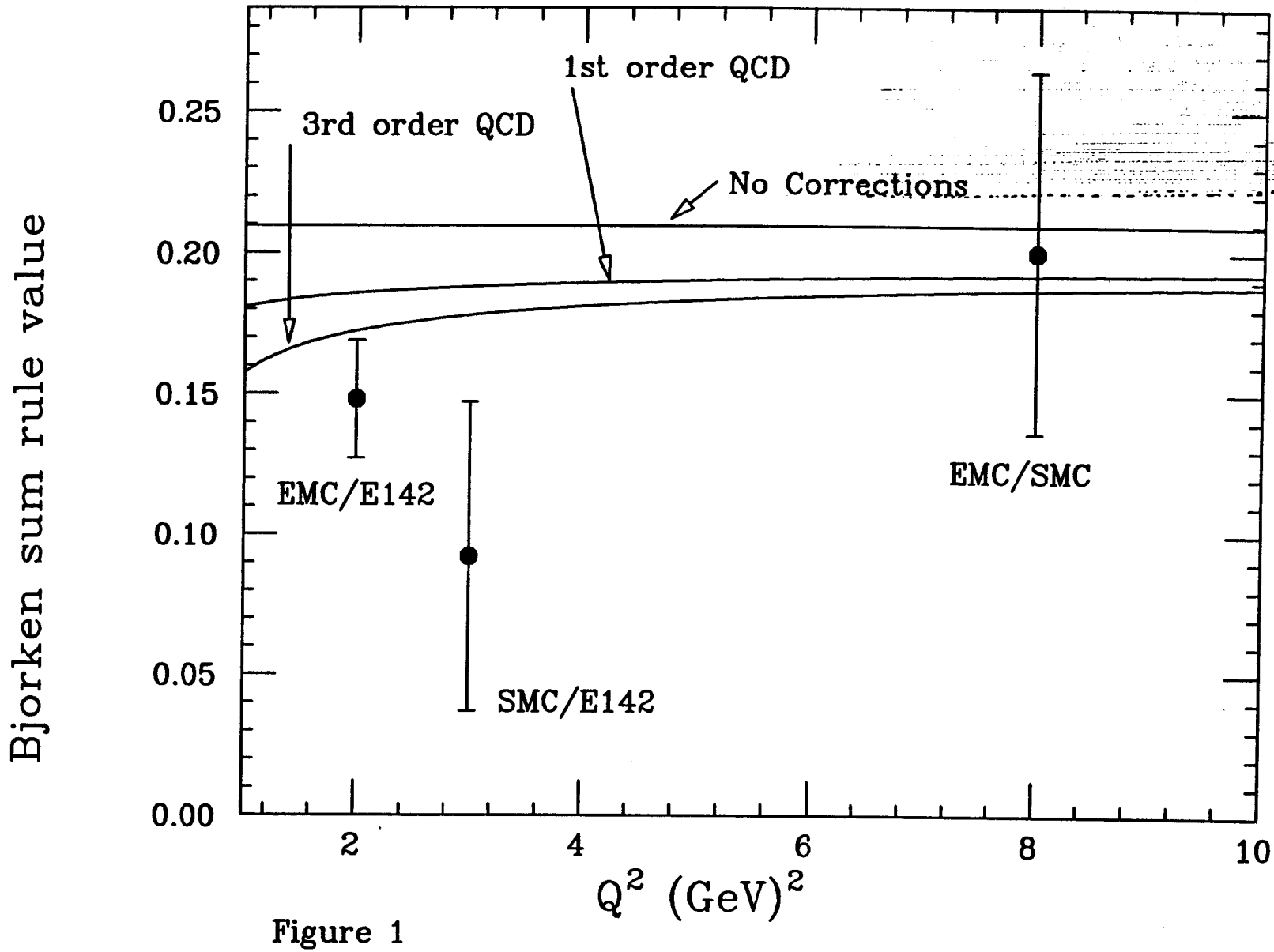
1st order QCD
3rd order QCD
No Corrections
EMC/E142
SMC/E142
EMC/SMC
Bjorken sum rule value
0.25
0.20
0.15
0.10
0.05
0.00
2
4
6
8
10
Q^2 (GeV)^2

Figure 1

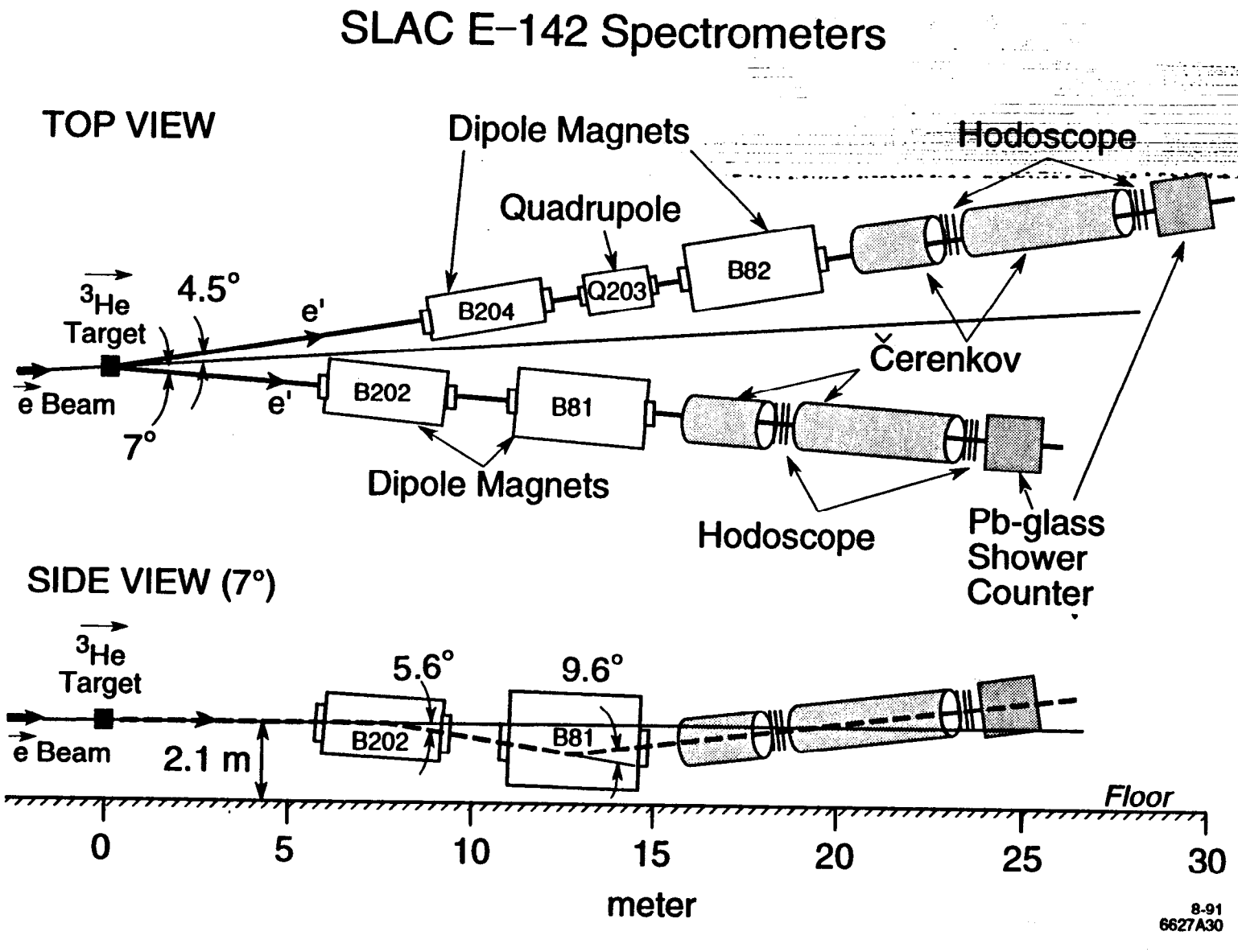
SLAC E-142 Spectrometers
TOP VIEW
Dipole Magnets
Hodoscope
Quadrupole
B82
Q203
B204
^{3}He
Target
4.5°
e'
e Beam
7°
e'
B202
B81
Čerenkov
Dipole Magnets
Hodoscope
Pb-glass
Shower
Counter
SIDE VIEW (7°)
^{3}He
Target
5.6°
9.6°
e Beam
2.1 m
B202
B81
Floor
0
5
10
15
20
25
30
meter
8-91
6627A30

FIGURE 2

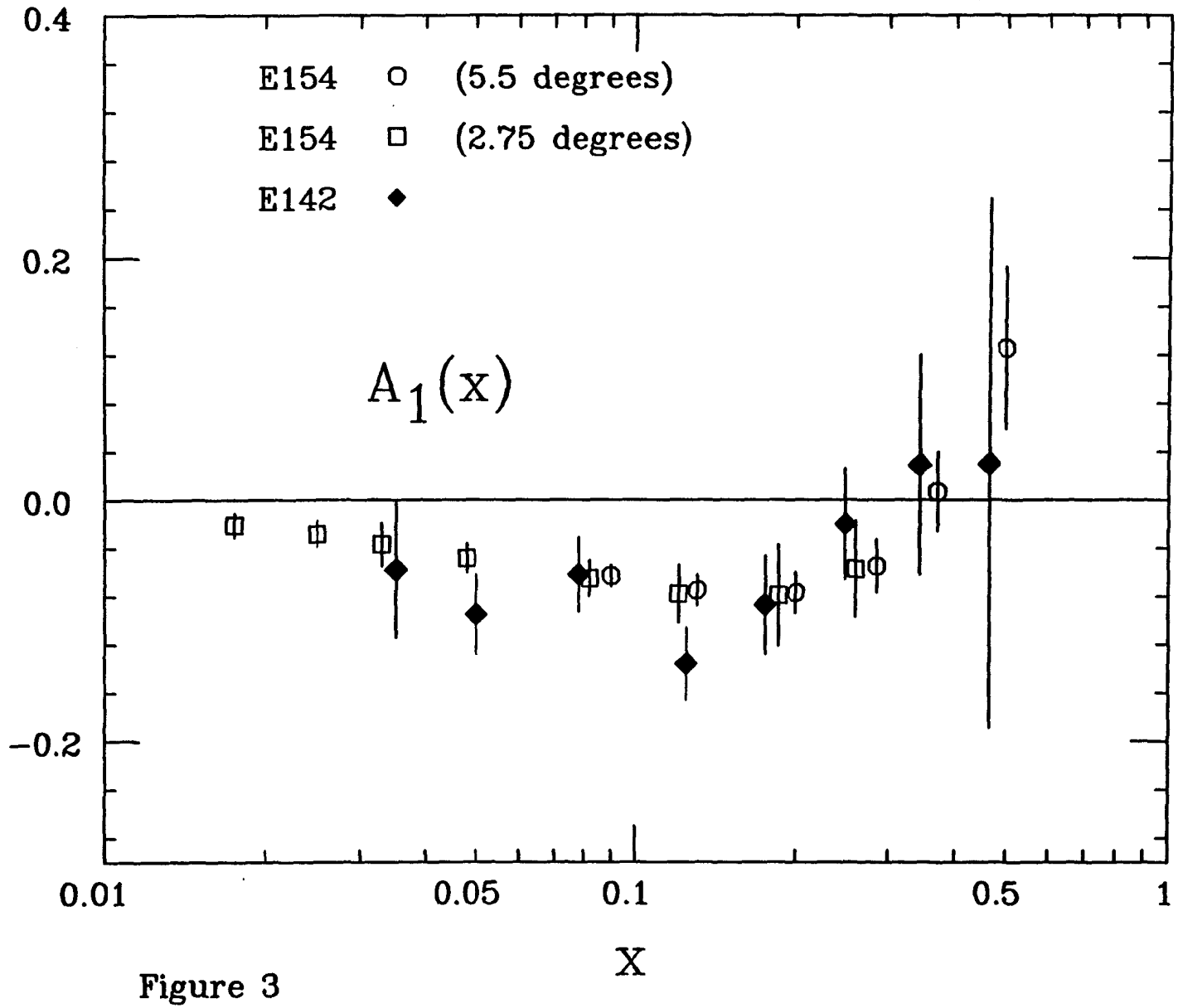
E154 (5.5 degrees)
E154 (2.75 degrees)
E142
$A_1(x)$
0.4
0.2
0.0
−0.2
0.01
0.05
0.1
0.5
1
X

Figure 3

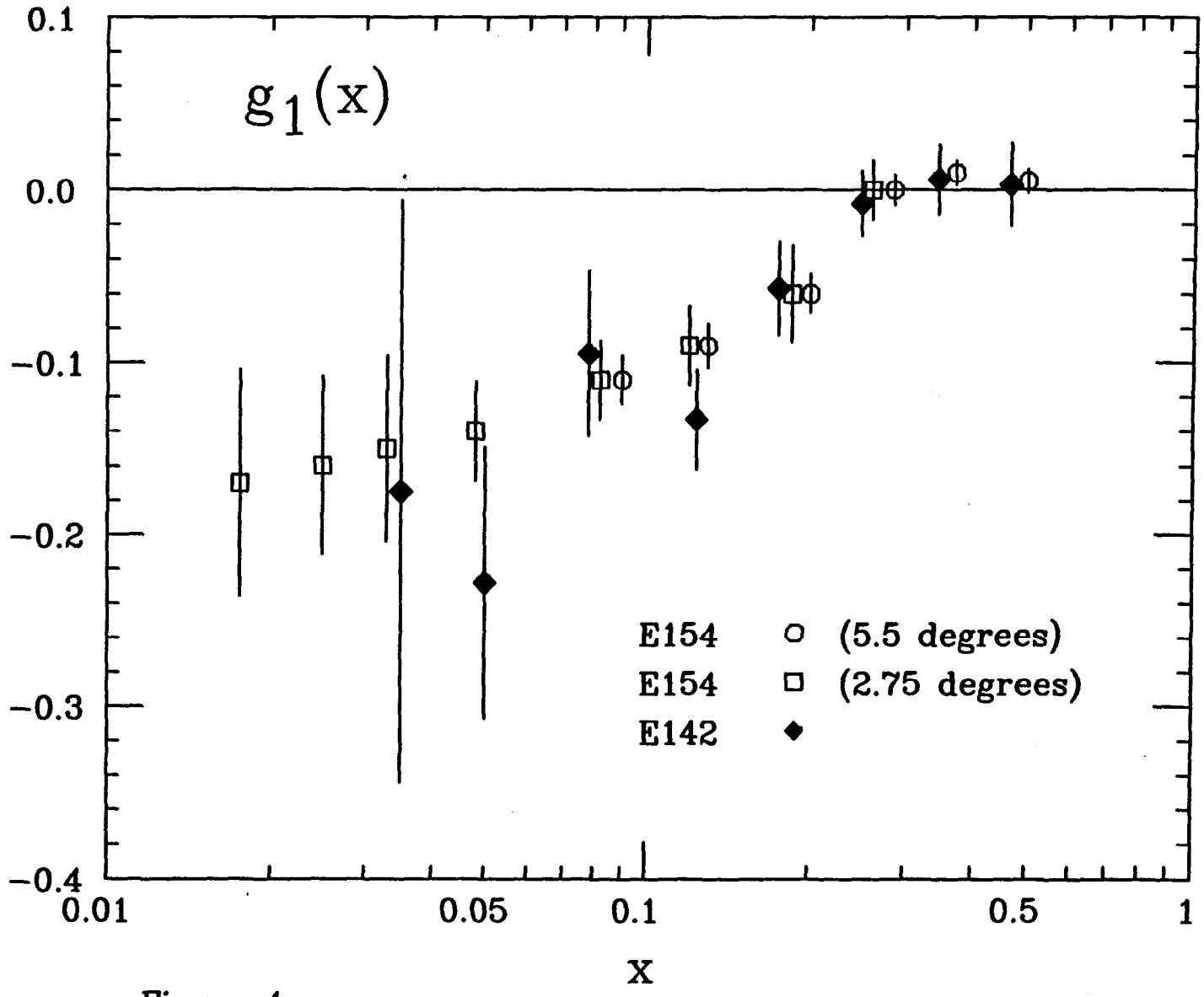
$g_1(x)$
0.1
0.0
−0.1
−0.2
−0.3
−0.4
0.01
0.05
0.1
0.5
1
x
E154 (5.5 degrees)
E154 (2.75 degrees)
E142

Figure 4

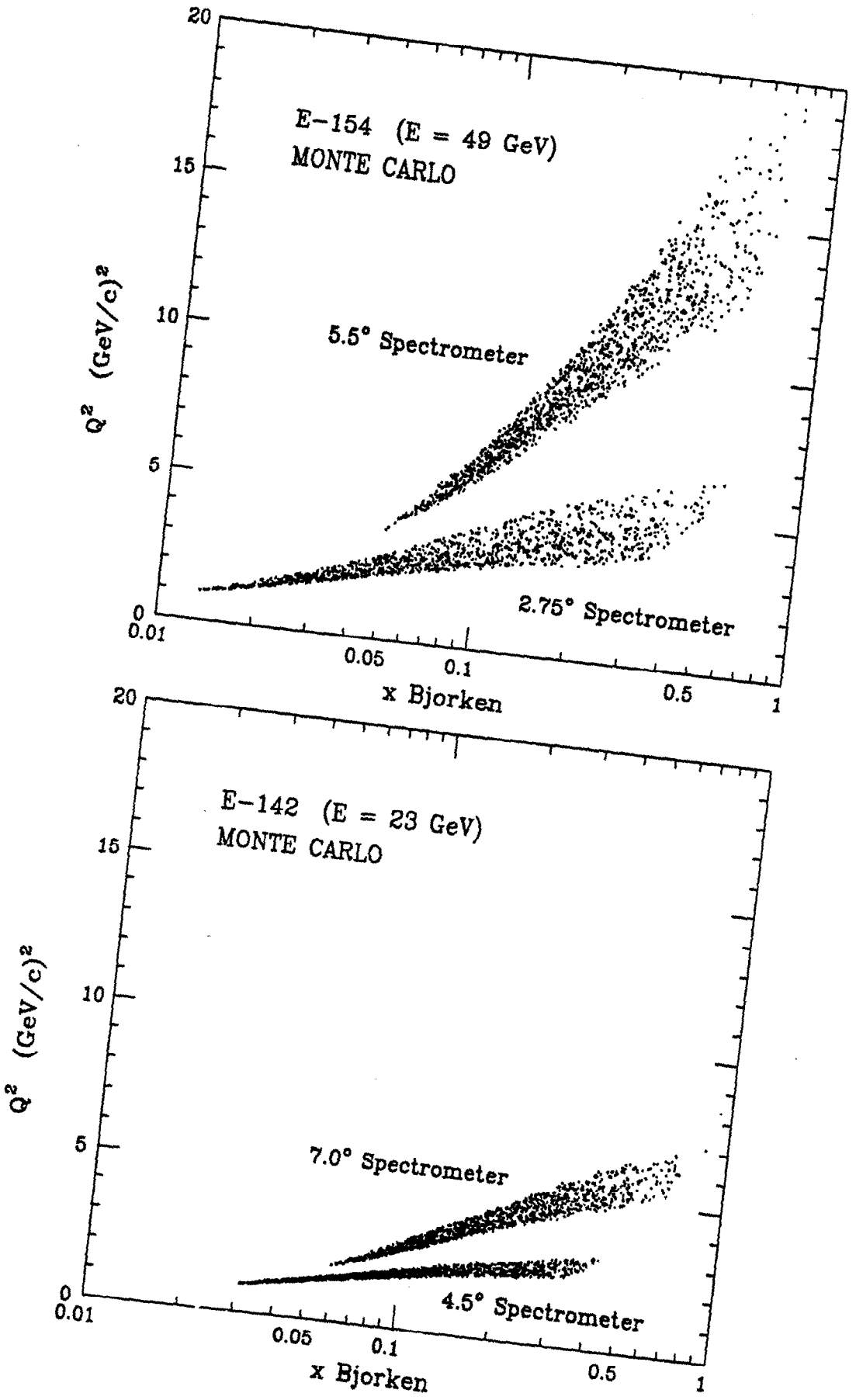
E−154 (E = 49 GeV)
MONTE CARLO
5.5° Spectrometer
2.75° Spectrometer
Q^2 (GeV/c)^2
x Bjorken
0
5
10
15
20
0.01
0.05
0.1
0.5
1
E−142 (E = 23 GeV)
MONTE CARLO
7.0° Spectrometer
4.5° Spectrometer
Q^2 (GeV/c)^2
x Bjorken

FIGURE 5

APPENDIX A

Determination of the quark spin distributions from the integrals over the nucleon structure functions

Four quantities from the quark parton model are of interest in understanding the nucleon spin distributions. These quantities are:

$$\Delta u,\ \Delta d,\ \Delta s$$

and the sum over the three:

$$\Delta q = \Delta u + \Delta d + \Delta s.$$

Δq and Δs give a measure of the amount of spin carried by the quarks and the strange sea, respectively. Each quark flavor parameter represents the integral over the difference in quark distributions in which the quark spin is aligned parallel versus anti-parallel to the spin of the nucleon:

$$\Delta q_i = \int_0^1 [q_i^{\uparrow}(x) - q_i^{\downarrow}(x)]dx$$

One can solve for Δu, Δd, and Δs assuming SU(6) [2] with the two following equations plus any one of the last three:

The Bjorken Sum Rule in the Quark Parton Model

$$\Delta u - \Delta d = \frac{g_A}{g_V}$$

Hyperon Decay

$$\Delta s - \Delta d = D - F$$

Spin Structure Functions in the Quark Parton Model

PROTON

$$\int_0^1 g_1^p(x) = \frac{4}{18}\Delta u + \frac{1}{18}\Delta d + \frac{1}{18}\Delta s$$

NEUTRON

$$\int_0^1 g_1^n(x) = \frac{4}{18}\Delta d + \frac{1}{18}\Delta u + \frac{1}{18}\Delta s$$

DEUTERON

$$\int_0^1 g_1^d(x) = \frac{5}{18}\Delta u + \frac{5}{18}\Delta d + \frac{2}{18}\Delta s$$

Therefore, with a measurement of the integral from either the proton, neutron or deuteron, one can determine the quark spin distributions (Δu, Δd, and Δs).

APPENDIX B

VOLUME 71, NUMBER 7 PHYSICAL REVIEW LETTERS 16 AUGUST 1993

Determination of the Neutron Spin Structure Function

P. L. Anthony,[6] R. G. Arnold,[1] H. R. Band,[13] H. Borel,[4] P. E. Bosted,[1] V. Breton,[2] G. D. Cates,[9] T. E. Chupp,[7] F. S. Dietrich,[6] J. Dunne,[1] R. Erbacher,[11] J. Fellbaum,[1] H. Fonvieille,[2] R. Gearhart,[10] R. Holmes,[12] E. W. Hughes,[10] J. R. Johnson,[13] D. Kawall,[11] C. Keppel,[1] S. E. Kuhn,[8] R. M. Lombard-Nelsen,[4] J. Marroncle,[4] T. Maruyama,[10] W. Meyer,[10] Z.-E. Meziani,[11] H. Middleton,[9] J. Morgenstern,[4] N. R. Newbury,[9] G. G. Petratos,[10] R. Pitthan,[10] R. Prepost,[13] Y. Roblin,[2] S. E. Rock,[1] S. H. Rokni,[10] G. Shapiro,[3] T. Smith,[7] P. A. Souder,[12] M. Spengos,[1] F. Staley,[4] L. M. Stuart,[10] Z. M. Szalata,[1] Y. Terrien,[4] A. K. Thompson,[5] J. L. White,[1] M. Woods,[10] J. Xu,[12] C. C. Young,[10] and G. Zapalac[13]

(E142 Collaboration)

[1]*American University, Washington, D.C. 20016*
[2]*Laboratoire de Physique Corpusculaire, Institut Nationale de Physique Nucléaire et de Physique des Particules/Centre Nationale de la Recherche Scientifique, Université Blaise Pascal, F-63170 Aubière Cedex, France*
[3]*University of California and Lawrence Berkeley Laboratory, Berkeley, California 94720*
[4]*Département de Physique Nucléaire, Centre d' Etudes Nucléaire de Saclay, F-91191 Gif-sur-Yvette Cedex, France*
[5]*Harvard University, Cambridge, Massachusetts 02138*
[6]*Lawrence Livermore National Laboratory, Livermore, California 94550*
[7]*University of Michigan, Ann Arbor, Michigan 48109*
[8]*Old Dominion University, Norfolk, Virginia 23529*
[9]*Princeton University, Princeton, New Jersey 08544*
[10]*Stanford Linear Accelerator Center, Stanford, California 94309*
[11]*Stanford University, Stanford, California 94305*
[12]*Syracuse University, Syracuse, New York 13210*
[13]*University of Wisconsin, Madison, Wisconsin 53706*

(Received 1 April 1993)

The spin structure function of the neutron g_1^n has been determined over the range $0.03 < x < 0.6$ at an average Q^2 of 2 $(\mathrm{GeV}/c)^2$ by measuring the asymmetry in deep inelastic scattering of polarized electrons from a polarized ^{3}He target at energies between 19 and 26 GeV. The integral of the neutron spin structure function is found to be $\int_0 g_1^n(x)dx = -0.022 \pm 0.011$. Earlier reported proton results together with the Bjorken sum rule predict $\int_0 g_1^n(x)dx = -0.059 \pm 0.019$.

PACS numbers: 13.60.Hb, 13.88.+e, 14.20.Dh, 25.30.Fj

For the past twenty years, results from deep inelastic scattering of polarized electrons and muons by polarized protons have been used to study the internal spin structure of the nucleon [1–3]. These experiments found large asymmetries over a large kinematic range as predicted by the quark-parton model (QPM). However, when interpreted by theoretical sum rules as described below, the data indicate that only a small fraction of the proton spin is carried by the quarks and that the strange sea polarization is large and negative. A complete understanding of nucleon spin structure requires information from neutron as well as more precise proton measurements. In this Letter we report new measurements of the neutron spin structure function g_1^n using longitudinally polarized electron scattering from a polarized ^{3}He target in End Station A at SLAC.

The spin structure functions G_1 and G_2 can be determined experimentally by measuring the difference in cross sections of polarized electrons on polarized nucleons between states where the spins are parallel and antiparallel [4,5],

$$\frac{d^2\sigma^{\uparrow\downarrow}}{dQ^2 d\nu} - \frac{d^2\sigma^{\uparrow\uparrow}}{dQ^2 d\nu} = \frac{4\pi\alpha^2}{Q^2 E^2}\left[M(E+E'\cos\theta)G_1(Q^2,\nu) - Q^2 G_2(Q^2,\nu)\right]. \quad (1)$$

Here M is the mass of the nucleon, ν is the electron energy loss, $q^2 = -Q^2$ is the square of the four-momentum of the virtual photon, α is the fine structure constant, E' is the scattered electron energy, E is the incident electron energy, θ is the electron scattering angle, and $d^2\sigma^{\uparrow\downarrow}$ $(d^2\sigma^{\uparrow\uparrow})$ is the differential scattering cross section for longitudinal target spins parallel (antiparallel) to the incident electron spins. A corresponding relationship exists for scattering of longitudinally polarized electrons off a transversely polarized target [5]. In the scaling limit (ν and Q^2 large), these structure functions are predicted to depend only on $x = Q^2/2M\nu$ yielding $M^2\nu G_1(\nu,Q^2) \to g_1(x)$ and $M\nu^2 G_2(\nu,Q^2) \to g_2(x)$.

Bjorken [6] developed a sum rule relating the integrals over the proton and neutron spin structure functions to the weak coupling constants g_A and g_V found in nucleon β decay:

$$\int_0^1 [g_1^p(x) - g_1^n(x)]dx = \frac{1}{6}\frac{g_A}{g_V}[1 - a_s(Q^2)/\pi], \quad (2)$$

where $a_s(Q^2)$ is the QCD coupling constant [7,8] and $g_A/g_V = 1.257 \pm 0.003$ [9]. The sum rule, first derived from current algebra, is a rigorous prediction of QCD. Ellis and Jaffe [10] have derived similar sum rules for the proton and neutron based on SU(3) symmetry and the

assumption that the strange sea is unpolarized:

$$\int_0^1 g_1^{p(n)}(x)dx = \tfrac{1}{18}[9(6)F-1(4)D][1-a_s(Q^2)/\pi]. \quad (3)$$

The constants F and D are SU(3) invariant matrix elements of the axial vector current where for neutron beta decay, $F+D=g_A/g_V$ [11]. The integral over the spin structure functions has a simple interpretation in the QPM:

$$\int_0^1 g_1^{p(n)}(x)dx = \tfrac{1}{2}[\tfrac{4}{9}\Delta u(d)+\tfrac{1}{9}\Delta d(u)+\tfrac{1}{9}\Delta s][1-a_s(Q^2)/\pi], \quad (4)$$

where Δu, Δd, and Δs represent the integral over the quark momentum distributions of the up, down, and strange quarks of the proton defined by

$$\Delta q = \int_0^1 [q^{\uparrow}(x)-q^{\downarrow}(x)]dx,$$

where $q^{\uparrow}(x)$ $[q^{\downarrow}(x)]$ are the quark plus antiquark momentum distributions for quark and antiquark spins parallel [antiparallel] to the nucleon spin. From SU(3) symmetry, the integral over the quark momentum distributions can be related to F and D via $\Delta d-\Delta s=F-D$. In the QPM, the Bjorken sum rule reduces to $\Delta u-\Delta d=F+D$. The European Muon Collaboration (EMC), which provided the first data for $x<0.1$, has reported a value

$$\int_0^1 g_1^p(x)dx = 0.126\pm0.010(\text{stat})\pm0.015(\text{syst})$$

for the proton integral [3], which is smaller than the value 0.175 ± 0.018 [11] from Eq. (3). In the QPM this result can be interpreted to mean that the total quark contribution to the proton spin is small ($\Delta u+\Delta d+\Delta s=0.13\pm0.19$), whereas the strange sea contribution is large and negative ($\Delta s=-0.16\pm0.08$).

The experimental quantities used to determine the spin structure functions are the two asymmetries:

$$A^{\parallel}=\frac{d\sigma^{\uparrow\downarrow}-d\sigma^{\uparrow\uparrow}}{d\sigma^{\uparrow\downarrow}+d\sigma^{\uparrow\uparrow}},\quad A^{\perp}=\frac{d\sigma^{\uparrow\leftarrow}-d\sigma^{\uparrow\rightarrow}}{d\sigma^{\uparrow\leftarrow}+d\sigma^{\uparrow\rightarrow}}. \quad (5)$$

Here $d\sigma^{\uparrow\leftarrow}$ ($d\sigma^{\uparrow\rightarrow}$) is the scattering cross section for beam spin antiparallel (parallel) to the beam momentum and target spin direction transverse to the beam momentum and towards the direction of the scattered electron, and $d\sigma^{\uparrow\downarrow}$ ($d\sigma^{\uparrow\uparrow}$) is defined in Eq. (1). The experimental asymmetries $A^{\parallel}$ and $A^{\perp}$ are related to the virtual photon-nucleon longitudinal and transverse symmetries, A_1 and A_2, respectively, via $A^{\parallel}=D(A_1+\eta A_2)$ and $A^{\perp}=d(A_2-\zeta A_1)$, where $D=(1-E'\epsilon/E)/(1+\epsilon R)$, $\eta=\epsilon\sqrt{Q^2}/(E-E'\epsilon)$, $d=D\sqrt{2\epsilon/(1+\epsilon)}$, $\zeta=\eta(1+\epsilon)/2\epsilon$, and $1/\epsilon=1+2[1+(\nu^2/Q^2)]\tan^2(\theta/2)$. Here R is the ratio of longitudinal to transverse virtual photoabsorption cross sections. The neutron spin structure function is extracted via

$$g_1^n=[A_1^nF_1^n+A_2^nF_1^n(2Mx/\nu)^{1/2}]/(1+2Mx/\nu),$$

where F_1^n is the spin averaged structure function of the neutron.

The SLAC polarized electron beam was created by photoemission from an AlGaAs photocathode [12] illuminated by a flash lamp pumped dye laser [13]. The polarized source delivered between 0.5 and 2.0×10^{11} electrons per pulse at 120 Hz. The pulse length varied from 0.8 to 1.4 μsec. The electron helicity was reversed randomly on a pulse-to-pulse basis by reversing the source laser circular polarization. Frequent helicity reversal is important because it avoids the introduction of false asymmetries from drifts in the operation of the beam, target, or spectrometers. The beam polarization was measured by a single-arm Møller polarimeter and was observed to be very stable and constant over the full run with an average value of $(38.8\pm1.6)\%$. The largest uncertainty arises from the measurement of the magnetization of the Møller target foils.

The ^{3}He nuclei in the gas target were polarized through spin-exchange collisions with optically pumped rubidium vapor. A two-chambered design was used [14] (Fig. 1). The target chamber had a length of 30 cm with 0.012 cm thick end windows and operated with a ^{3}He density of 2.3×10^{20} atoms/cm^3 (8.6 atm at 0°C). A small amount of nitrogen ($\sim1.9\times10^{18}$ atoms/cm^3) increased the optical pumping efficiency. Five high-power laser systems produced 20 W cw of near infrared laser light for optical pumping. The ^{3}He polarization was measured with NMR techniques with an uncertainty of $\Delta P_t/P_t$ of 7%. The largest contribution came from the uncertainty in the NMR calibration measurements of the thermal equilibrium polarization of protons in water. P_t varied slowly between 30% and 40% during the experiment; its direction was reversed frequently to cancel systematic false asymmetries.

Data were collected at three different beam energies, 19.4, 22.7, and 25.5 GeV covering a range in x from 0.03 to 0.6 with Q^2 greater than 1 $(\text{GeV}/c)^2$. The total event sample amounted to $\sim4\times10^8$ electrons collected in two single-arm magnetic spectrometers [15], at horizontal scattering angles of 4.5° and 7° (Fig. 2). The detectors in each spectrometer consisted of two N_2 threshold Čerenkov counters, six planes of hodoscopes, and a 24 radiation length shower counter composed of 200 lead glass blocks. Each spectrometer accepted charged particles with momenta greater than ~6 GeV/c. The momentum resolution (rms) from hodoscope tracking was $\Delta E'/E'\sim3\%$ on average, and the shower energy resolution was typically $15\%/\sqrt{E'\,(\text{GeV})}$.

The experimental asymmetry $A^{\parallel}$ is derived from the measured raw counting rate asymmetry $\Delta=(N^{\uparrow\downarrow}-N^{\uparrow\uparrow})/(N^{\uparrow\downarrow}+N^{\uparrow\uparrow})=A^{\parallel}P_tP_bf$ where $N^{\uparrow\uparrow}$ and $N^{\uparrow\downarrow}$ represent the number of scattered electrons per incident beam electron in the spectrometer when the beam and target spins are parallel and antiparallel, respectively. Here, P_t and P_b are the target and beam polarizations. The dilution factor f is the fraction of events originating

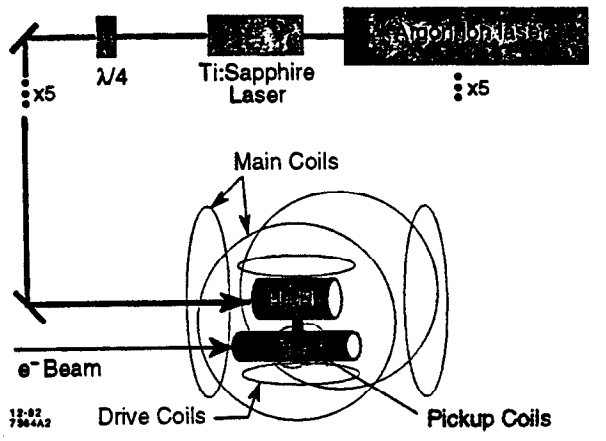

FIG. 1. Schematic layout of the polarized ^{3}He target. Five sets of lasers optically pump rubidium vapor in the top chamber for polarization of ^{3}He nuclei. Incident electrons scatter off the nuclei in the bottom chamber. Two sets of Helmholtz coils hold the target spins in the longitudinal or transverse direction. Drive and pickup coils are used to measure polarization.

from polarized neutrons in the target ($f \sim 0.11 \pm 0.02$ and varies slowly with x). All counting rates were corrected for deadtime and normalized to the total incident charge as measured by two independent toroidal charge monitors. Beam charge differences between parallel and antiparallel polarized electrons were measured to be on the order of 1 part in 10^4.

Electrons were identified by a coincidence of the two Čerenkov counters and a large pulse height in the shower counter. Electron energy and position in the shower counter determined the x and Q^2 of the event. Hodoscope tracking was used for systematic studies and for the absolute energy calibration of the lead glass. The electron background from charge-symmetric processes was determined to be $\sim 5\%$ of the electron sample at low x by measuring the positron rate in runs with the spectrometer magnet polarity reversed. The background from misidentified pions was studied using a comparison of momentum from tracking to shower energy deposition and contributed about 2% to the electron sample at low x. Contaminations in the high x bins were negligible. Glass cell runs with variable pressures of ^{3}He were used to study the dilution factor by separating contributions from scattering off ^{3}He versus glass. The largest systematic

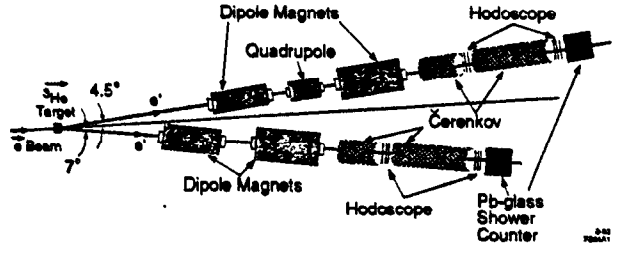

FIG. 2. Layout of the experimental setup. Two independent single-arm spectrometers are shown.

uncertainty in this experiment comes from the determination of the dilution factor to $\pm 15\%$ of its value. False asymmetries were found to be consistent with zero by comparing data with target spins in opposite directions.

Internal spin-dependent radiative corrections were calculated using the complete Kukhto and Shumeiko formulas [16] (exact integration, no peaking approximation). External radiative corrections followed Mo and Tsai [17], but were small because the target was thin ($\sim 0.3\%$ radiation length). The total corrections amounted to a relative change in the asymmetry ranging from $(30 \pm 15)\%$ at low x to $(5 \pm 2)\%$ at high x. The uncertainty from the radiative corrections takes into account variations due to the model dependence on the corrections.

A polarized ^{3}He nucleus is regarded as a good model of a polarized neutron for deep inelastic scattering [18,19]. The ^{3}He wave function is primarily in an S-state in which the two protons pair with opposite spins due to the Pauli exclusion principle, leaving the neutron spin as the dominant contribution to spin-dependent scattering. A small correction from the polarization of the two protons in ^{3}He ($\sim -2.7\%$ per proton) and a correction for the polarization of the neutron in ^{3}He ($\sim 87\%$) were applied in order to extract the neutron asymmetry from the measured ^{3}He asymmetry [20,21]. For the proton correction, the asymmetry results from EMC were taken [3]. No other corrections were made because of the fact that the polarized neutron is embedded in the ^{3}He nucleus.

The physics asymmetry A_1^n vs x is presented in Fig. 3. Since no significant Q^2 dependence of the measurements was observed, the data at different energies for fixed x bins are averaged over Q^2. A clear trend of negative asymmetries is evident. Measurements of the transverse neutron asymmetry A_2^n were found to be consistent with zero with statistical uncertainties of typically ± 0.25. The lower part of Fig. 3 shows the neutron spin structure function extracted from the measured asymmetries, using the results from a global fit to SLAC structure function data [22].

The integral of the spin structure function over the measured range of x is

$$\int_{0.03}^{0.6} g_1^n(x)dx = -0.019 \pm 0.007(\text{stat}) \pm 0.006(\text{syst})$$

at an average Q^2 of 2 $(\text{GeV}/c)^2$. Propagating the unpolarized structure function to Q^2 of 2 $(\text{GeV}/c)^2$ for all x bins gives the same result. Extrapolation of the spin structure function outside the measured x range requires models of the neutron spin structure. Assuming perturbative QCD, the asymmetry A_1^n approaches 1 as x approaches 1. Using this constraint and a Regge parametrization ($A_1^n \sim x^{1.2}$) to fit the low x data [23], the neutron integral is extracted over the full x range, $\int_0^1 g_1^n(x)dx = -0.022 \pm 0.011$. The extrapolations to low and high x amounted to additions to the measured integral of -0.006 ± 0.006 and 0.003 ± 0.003, respectively. Combining the integral over the neutron spin structure func-

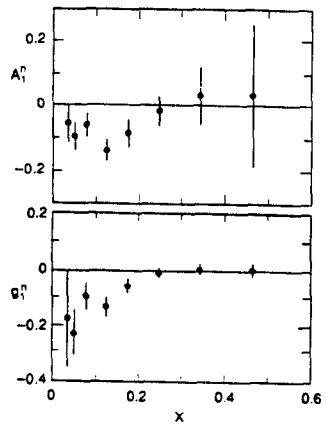

FIG. 3. Results for neutron asymmetries A_1^n and the neutron spin structure function g_1^n as a function of x averaged over Q^2. Statistical and systematic errors are added in quadrature.

tion from this experiment with the proton integral from EMC [3] corrected to Q^2 of 2 $(\mathrm{GeV}/c)^2$ gives the integral $\int_0^1 [g_1^p(x) - g_1^n(x)]dx = 0.146 \pm 0.021$. This is to be compared to a Bjorken sum rule prediction of 0.183 ± 0.007 using $\alpha_s = 0.39 \pm 0.10$ at Q^2 of 2 $(\mathrm{GeV}/c)^2$. Higher order QCD corrections [24] or higher twist effects [25] may account for the apparent discrepancy.

The results from this experiment in conjunction with the weak coupling constants from baryon decay, $F = 0.47 \pm 0.04$ and $D = 0.81 \pm 0.03$ [11], can be used to extract the integral over the quark spin distributions from the QPM using $\alpha_s = 0.385$ at Q^2 of 2 $(\mathrm{GeV}/c)^2$. The results yield $\Delta u = 0.93 \pm 0.06$, $\Delta d = -0.35 \pm 0.04$, and $\Delta s = -0.01 \pm 0.06$. These results imply that the total quark contribution to the nucleon spin $(\Delta u + \Delta d + \Delta s)$ is 0.57 ± 0.11. Thus, the quarks contribute approximately one-half of the nucleon spin, and the strange sea contribution is small. Orbital angular momentum [26] and the spin of the gluons [27] may account for the remaining nucleon spin.

A new measurement on the deuteron by the Spin Muon Collaboration combined with the EMC proton result leads to a neutron integral of $-0.08 \pm 0.04(\mathrm{stat}) \pm 0.04(\mathrm{syst})$ [28]. Within the 6 times larger error, this result is consistent with ours.

We have presented results on the neutron spin structure function and used them to test QCD sum rules. When combined with the proton results from EMC, the results from this experiment differ from the Bjorken sum rule prediction evaluated to first order in α_s by ~ 2 standard deviations. Within present theoretical uncertainties on the corrections to the Bjorken sum rule, the discrepancy is of marginal significance. Our results give a reasonable QPM interpretation and good agreement with the updated value of the Ellis-Jaffe sum rule [11] $\int_0^1 g_1^n(x)dx = -0.021 \pm 0.018$ at a Q^2 of 2 $(\mathrm{GeV}/c)^2$. The striking difference between the EMC QPM interpretation and ours is at the same 2-standard-deviation level as the Bjorken sum rule difference. More precise proton data can help resolve whether the 2-standard-deviation problem is real and clarify the QPM interpretation.

This work was supported by Department of Energy Contracts No. DE-AC03-76SF0900098 (LBL), No. W-2705-Eng-48 (LLNL), No. DE-FG02-90ER40557 (Princeton), No. DE-AC03-76SF00515 (SLAC), No. DE-FG03-88ER40439 (Stanford), No. DE-FG02-84-ER40146 (Syracuse), and No. DE-AC02-76ER00881 (Wisconsin), and National Science Foundation Grants No. 9014406, No. 9114958 (American), No. 8914353, No. 9200621 (Michigan), and the Bundesministerium für Forschung und Technologie (W.M.).

[1] M. J. Alguard *et al.*, Phys. Rev. Lett. **37**, 1258 (1976); **37**, 1261 (1976).
[2] G. Baum *et al.*, Phys. Rev. Lett. **51**, 1135 (1983).
[3] J. Ashman *et al.*, Phys. Lett. B **206**, 364 (1988); Nucl. Phys. **B328**, 1 (1989).
[4] C. E. Carlson and W.-K. Tung, Phys. Rev. D **5**, 721 (1972).
[5] A. J. G. Hey and J. E. Mandula, Phys. Rev. D **5**, 2610 (1972).
[6] J. D. Bjorken, Phys. Rev. **148**, 1467 (1966); Phys. Rev. D **1**, 1376 (1970).
[7] J. Kodaira *et al.*, Phys. Rev. D **20**, 627 (1979).
[8] J. Kodaira *et al.*, Nucl. Phys. **B159**, 99 (1979); **B165**, 129 (1980).
[9] Particle Data Group, Review of Particle Properties, Phys. Rev. D **45**, 1 (1992).
[10] J. Ellis and R. Jaffe, Phys. Rev. D **9**, 1444 (1974).
[11] R. L. Jaffe and A. V. Manohar, Nucl. Phys. **B337**, 509 (1990).
[12] T. Maruyama *et al.*, J. Appl. Phys. **73**, 5189 (1993).
[13] M. Woods *et al.*, Report No. SLAC-PUB-5965, 1992 (unpublished).
[14] T. E. Chupp *et al.*, Phys. Rev. C **45**, 915 (1992); **36**, 2244 (1987).
[15] G. G. Petratos *et al.*, Report No. SLAC-PUB-5678, 1991 (unpublished).
[16] T. V. Kukhto and N. M. Shumeiko, Nucl. Phys. **B219**, 412 (1983).
[17] L. W. Mo and Y. S. Tsai, Rev. Mod. Phys. **41**, 205 (1969).
[18] R. M. Woloshyn, Nucl. Phys. **496A**, 749 (1989).
[19] C. Ciofi degli Atti *et al.*, University of Perugia Report No. DFUPG-75/93 (to be published).
[20] B. Blankleider and R. M. Woloshyn, Phys. Rev. C **29**, 538 (1984).
[21] J. L. Friar *et al.*, Phys. Rev. C **42**, 2310 (1990).
[22] L. W. Whitlow *et al.*, Phys. Lett. B **250**, 193 (1990); **282**, 475 (1992).
[23] A. Schafer, Phys. Lett. B **208**, 175 (1988).
[24] S. A. Larin and J. A. M. Vermaseren, Phys. Lett. B **259**, 345 (1991).
[25] I. I. Balitsky *et al.*, Phys. Lett. B **242**, 245 (1990).
[26] J. Ellis and M. Karliner, Phys. Lett. B **213**, 73 (1988).
[27] G. Altarelli and G. G. Ross, Phys. Lett. B **212**, 391 (1988).
[28] B. Adeva *et al.*, Phys. Lett. B **362**, 553 (1993).

SLAC-PUB-5678
October 1991
(E)

APPENDIX C

Large Acceptance Magnetic Spectrometers for Polarized Deep Inelastic Electron Scattering*

G. G. Petratos, R. L. Eisele, R. A. Gearhart, E. W. Hughes, and C. C. Young
Stanford Linear Accelerator Center, Stanford University, Stanford, CA 94309

Abstract

The design of two magnetic spectrometers for the measurement of the spin-dependent structure function g_1^n of the neutron and a test of the Bjorken sum rule is described. The measurement will consist of scattering 23 GeV polarized electrons off a polarized ^{3}He target and detecting scattered electrons of 7 to 18 GeV at 4.5° and 7°. Each spectrometer is based on two large aperture dipole magnets bending in opposite directions. This "reverse" deflection design doubles the solid angle as compared to the conventional design of same direction bends used in previous experiments. Proper choice of the deflection angles and the distance between the two dipoles in each spectrometer allows background photons from radiative processes to reach the detectors only after at least two bounces off the spectrometer vacuum walls, resulting in an expected tolerable background. Each spectrometer is equipped with a pair of Čerenkov detectors, a pair of scintillation hodoscopes and a lead-glass shower calorimeter providing electron and pion identification with angular and momentum resolutions sufficient for the experimental measurement.

MOTIVATION

This paper describes the design of two magnetic spectrometers to be used in an experiment [1] at the Stanford Linear Accelerator Center that will (a) measure the spin-dependent structure function $g_1^n(x)$ of the neutron in the Bjorken scaling variable x from 0.035 to 0.7 with squared four-momentum transfers $Q^2 > 1$ (GeV/c)^2 and (b) test the Bjorken polarization sum rule [2]:

$$\int_0^1 [g_1^p(x) - g_1^n(x)]dx = \frac{1}{6}\left|\frac{g_A}{g_V}\right|\left[1 - \frac{\alpha_s(Q^2)}{\pi}\right], \qquad (1)$$

where $g_1^p(x)$ is the proton spin-dependent structure function, α_s is the QCD coupling constant and $|g_A/g_V|$ is the ratio of the axial to vector weak coupling constants in the nucleon beta decay. The experiment is also expected to provide valuable information in understanding the violation of the Ellis-Jaffe quark parton model sum rule [3] as measured by the EMC collaboration [4].

THE EXPERIMENT

The experiment consists of scattering a 22.7 GeV longitudinally polarized electron beam off a polarized ^{3}He (neutron) target [5] and detecting scattered electrons in two magnetic spectrometer systems. The neutron spin structure function g_1^n is proportional to the difference over the sum of the scattering cross sections in which the beam and target polarizations are parallel versus anti-parallel. The beam polarization will be measured by means of a Møller polarimeter [6] and the target polarization by two NMR techniques [5,7].

THE MAGNET SYSTEMS

The two spectrometers will be centered around 4.5° and 7.0°, which are the optimum scattering angles corresponding to the maximum polarized electron beam energy of 22.7 GeV, presently available at the SLAC fixed target End Station A facility. A momentum acceptance ranging from 7 to 18 GeV/c is required at these angles to cover the desired range in the Bjorken x scaling variable from 0.035 to 0.7. A schematic of the two systems is shown in Fig. 1. Both systems use magnetic elements from the SLAC 8 and 20 GeV/c spectrometers and standard surplus concrete blocks for background shielding.

The design of the two systems was driven by several requirements. The cross sections to be measured are known to be small, typically of the order of 10^{-32} cm^2/(sr·GeV). The asymmetry in the cross sections of the two different spin orientations is also predicted to be small, of the order of 10^{-3}. In order to minimize beam running time, the spin structure function measurements require spectrometers with the largest possible solid angle over a momentum acceptance range extending from 7 to 18 GeV/c.

In addition, these small scattering angle spectrometers should be able to suppress an expected large photon background coming from the target due to bremsstrahlung radiation, radiative Møller scattering and the decay of photoproduced π^0 mesons. Background rate estimates [8] have indicated the need for at least a "two bounce system" (the shape of the spectrometer aperture should allow a photon to reach the detectors only after bouncing twice on the magnet gaps or vacuum walls) in order to keep this background at a tolerable level.

The momentum resolution of the spectrometers is defined solely by the required x resolution. The cross section asymmetries are not expected to exhibit any sizable dependence on momentum transfer [4]. A resolution in x ranging from ±0.004 at x=0.035 to ±0.07 at x=0.7 ($\Delta x/x$ = ±0.10) is considered adequate for the needs of the asymmetry measurements. This translates to a required momentum resolution that varies from ±6.9% at E'=7 GeV/c to ±2.2% at E'=18 GeV/c for both spectrometers.

Past designs for polarized deep inelastic scattering experiments at SLAC [9,10] have achieved a solid angle

* Work supported by Department of Energy contracts DE-AC03-76SF00515.

Presented at the IEEE Nuclear Science Symposium and Medical Imaging Conference, Santa Fe, NM, November 5-9, 1991.

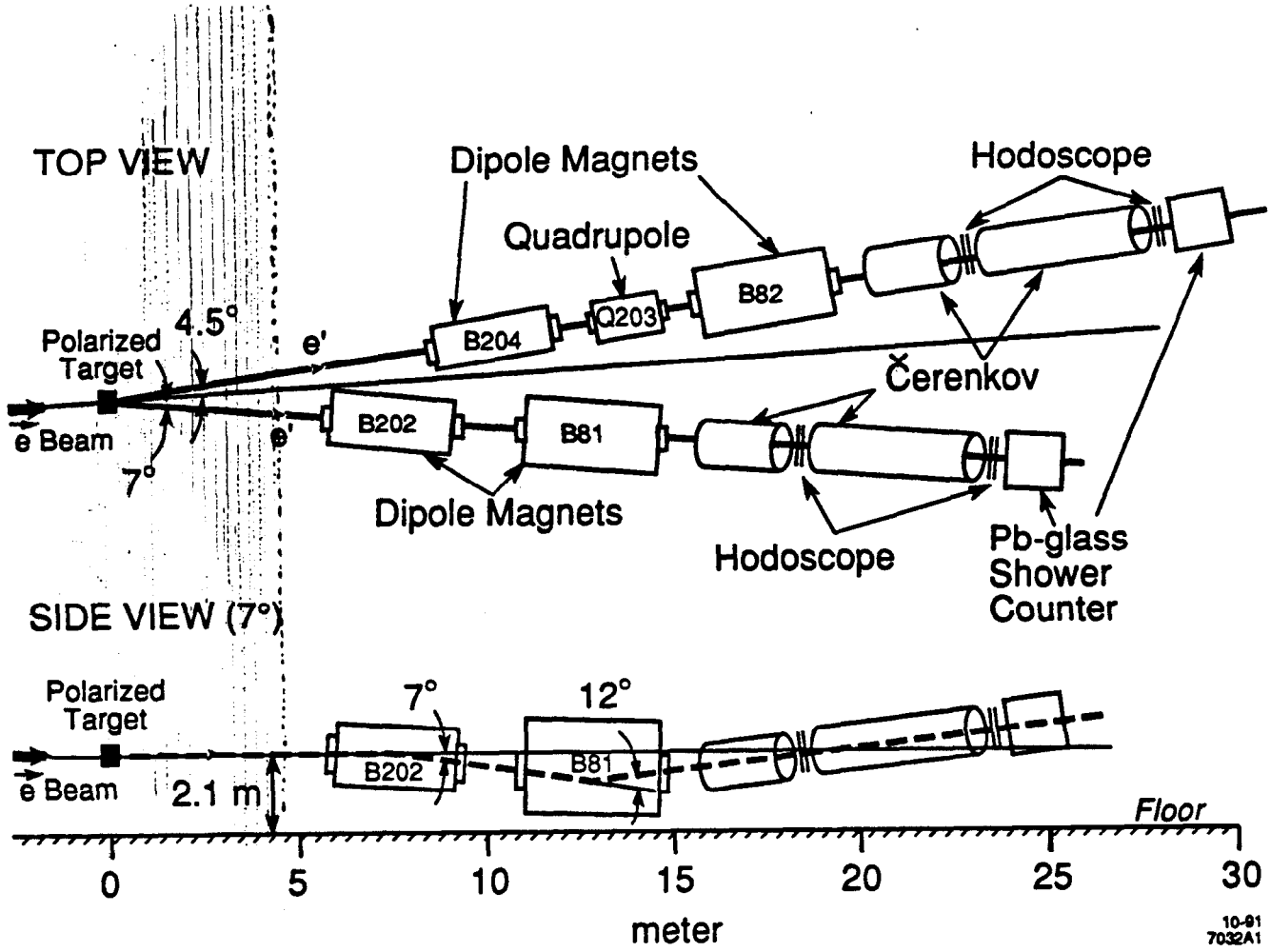

Fig. 1. The two magnetic spectrometer systems and detector packages. The dipoles B202 and B204 and the quadrupole Q203 are magnetic elements from the SLAC 20 GeV/c spectrometer. The dipoles B81 and B82 are elements from the SLAC 8 GeV/c spectrometer. Not shown is a set of wire chambers in the 4.5° arm and/or a third hodoscope in both arms (under consideration).

peaking at a maximum value of ~0.6 msr for the central momentum but falling rapidly on either side of the relative momentum. The designs were based on two large aperture dipole magnets both bending in the same direction. A new design with the two dipoles bending in opposite directions provides a solid angle peaking at the same maximum but remaining constant over a large momentum interval $\Delta E'/E' \sim 100\%$. The solid angle of the "reverse bend" dipole doublet configuration, when integrated over the 7 to 18 GeV/c momentum interval, is twice that of the "conventional" configuration. The solid angle of the two spectrometers is shown as a function of momentum in Figs. 2 and 3.

The reverse bend can also fulfill the "two bounce" requirement by properly choosing the deflecting angles and the separation of the two dipoles. In the 7.0° spectrometer the distance between the two dipoles was chosen to be 2 m and the two deflection angles 7° for B202 and 12° for B81. This combination makes the spectrometer a "two bounce" system for photons and at the same time provides sufficient total dispersion for determining the scattered particle momenta. In the 4.5° arm the deflection angles of the dipoles are the same as for the 7.0° arm but their separation is 4 m resulting in an almost "three bounce" system.

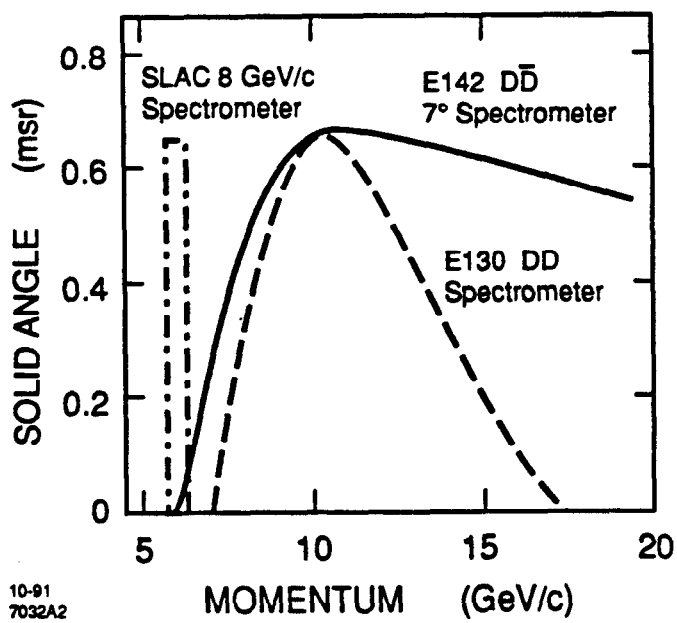

Fig. 2. The solid angle of the 7.0° magnetic spectrometer system plotted versus momentum. The acceptances of the E130 spectrometer and of the SLAC 8 GeV/c spectrometer are shown for comparison.

Resolutions

The shower counter resolution for electrons should be about $\sigma/E' \approx \pm 7\%/\sqrt{E'}$. This estimate will result in a energy resolution $< \pm 2.5\%$, adequate for the needs of this experiment. The counter will be calibrated with a sample of scattered electrons of known energy in special elastic electron-proton scattering runs using a gaseous hydrogen target. The energy of the scattered electrons in these runs will be ~ 5 GeV. Extrapolation of the calibration algorithm to higher energies will be checked using the scintillator hodoscopes.

The angular tracking resolutions of the hodoscopes are ± 0.7 mr for the 4.5° spectrometer and ± 0.9 mr for the 7.0° spectrometer; the position tracking resolutions are ± 0.3 cm for both spectrometers. The expected angular resolutions in the non-bend plane are $\sim \pm 0.3$ mr for both spectrometers. In the bend plane, they are $\sim \pm 0.9$ mr for the 4.5° arm and $\sim \pm 0.3$ mr for the 7° arm.

The momentum resolution depends on the absolute value of momentum and varies from $\pm 0.5\%$ to $\pm 1.8\%$ for the 4.5° spectrometer and from $\pm 0.6\%$ to $\pm 3.5\%$ for the 7.0° spectrometer as can be seen in Fig. 6. The figure also shows the projected energy resolution of the reconfigured ASP shower counter as well as the required momentum resolution that corresponds to the desired Bjorken x resolution. The angular and momentum spectrometer resolutions, averaged over the 7 to 18 GeV/c range, are given for both systems in Table 1.

The initial (at the target) production coordinates χ_o, θ_o, y_o and ϕ_o and the momentum of the particles transported through the spectrometers will be reconstructed by means of reverse-order TRANSPORT matrix elements [15] using the final (at the second hodoscope location) χ_f, θ_f, y_f and ϕ_f coordinates of the particles. The very large momentum bites of the spectrometers require at least a third-order reverse TRANSPORT expansion in y_f and ϕ_f for reconstructing the particle momenta as can be seen in Figs. 7 and 8. The angular coordinates θ_o and ϕ_o are well reconstructed by a second-order reverse expansion in terms of the final coordinates.

Summary and Outlook

The reverse bend design generally is a practical, efficient configuration for low resolution experiments that require high momentum (> 10 GeV/c) spectrometers maintaining a large solid angle over a large momentum range.

Another experiment using the two spectrometer systems is being proposed [16] at SLAC for measuring deep inelastic scattering of 25.9 GeV polarized electrons from polarized ammonia (NH_3) and deuterated ammonia (ND_3) targets. The same spectrometer design could be used in the polarized experiments possible with a planned [17] upgraded beam energy of 50 GeV.

Acknowledgments

We wish to acknowledge the invaluable support of Sylvia MacBride, Vani Bustamante and Kevin Johnston from the SLAC Publications Department in this work.

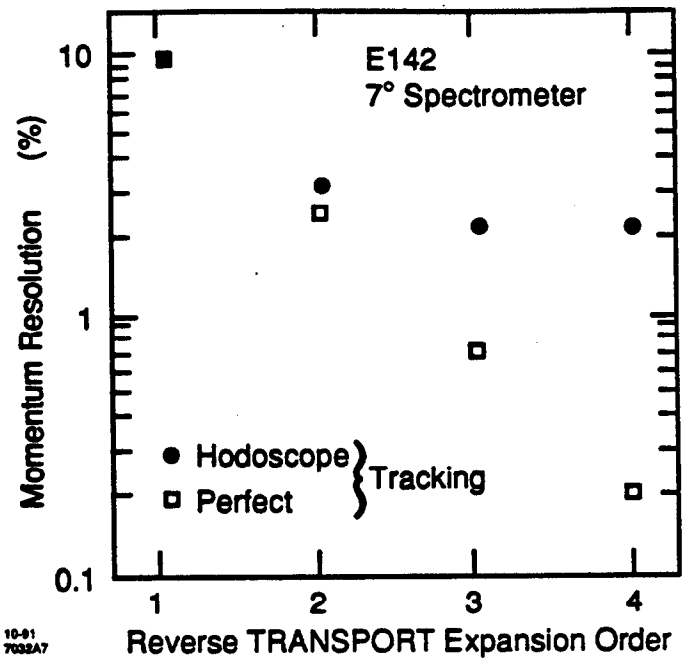

Fig. 7. Average momentum resolution of the 7° spectrometer system versus the order of the reverse TRANSPORT set of matrix elements. Shown is the intrinsic resolution assuming perfect tracking and the resolution using the track information from the two hodoscopes.

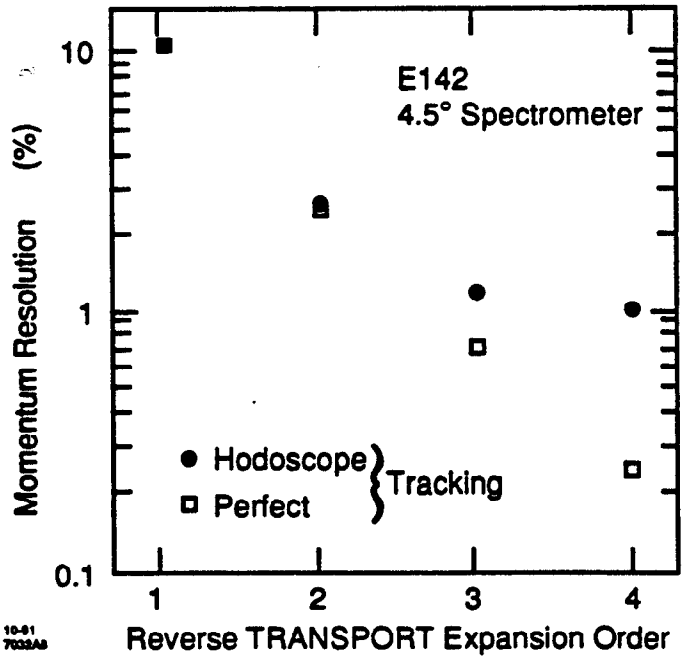

Fig. 8. Average momentum resolution of the 4.5° spectrometer system versus the order of the reverse TRANSPORT set of matrix elements. Shown is the intrinsic resolution assuming perfect tracking and the resolution using the track information from the two hodoscopes.

Table 1. Momentum and angular resolutions, averaged over a 7 to 18 GeV/c range, using third-order (second-order) reverse matrix elements for momentum (angle) reconstruction.

7° Spectrometer

RESOLUTION	Intrinsic	Hodoscope Tracking
Momentum	± 0.7 %	± 2.2 %
Bend Plane Angle ϕ_0	± 0.2 mr	± 0.3 mr
Non–bend Plane Angle θ_0	0 mr	± 0.3 mr

4.5° Spectrometer

RESOLUTION	Intrinsic	Hodoscope Tracking
Momentum	± 0.6 %	± 1.2 %
Bend Plane Angle ϕ_0	± 0.7 mr	± 0.9 mr
Non–bend Plane Angle θ_0	0 mr	± 0.3 mr

REFERENCES

[1] E. W. Hughes *et al.*, "SLAC Proposal E142: A Proposal to Measure the Neutron Spin-Dependent Structure Function" (1989).

[2] J. D. Bjorken, "Applications of the Chiral U(6)⊗U(6) Algebra of Current Densities," *Phys. Rev.* **148**, pp. 1467–1478, 1966; "Inelastic Scattering of Polarized Leptons from Polarized Nucleons," *Phys. Rev.* **D1**, pp. 1376–1379, 1970.

[3] J. Ellis and R. L. Jaffe, "A Sum Rule for Deep Inelastic Electroproduction for Polarized Protons," *Phys. Rev.* **D9**, pp. 1444–1446, 1974.

[4] J. Ashman *et al.*, "An Investigation of the Spin Structure of the Proton in Deep Inelastic Scattering of Polarized Muons on Polarized Protons," *Nucl. Phys.* **B328**, pp. 1–35, 1989.

[5] T. E. Chupp *et al.*, "Polarized, High-Density, Gaseous ^{3}He Targets," *Phys. Rev.* **C36**, pp. 2244–2251, 1987.

[6] H. R. Band, private communication.

[7] S. R. Schaefer *et al.*, "Frequency Shifts of the Magnetic-Resonance Spectrum of Mixtures of Nuclear Spin-Polarized Noble Gases and Vapors of Spin-Polarized Alkali-Metal Atoms," *Phys. Rev.* **A39**, pp. 5613–5623, 1989.

[8] Z-E. Meziani, private communication.

[9] C. Y. Prescott *et al.*, "Parity Nonconservation in Inelastic Electron Scattering," *Phys. Lett.* **B77**, pp. 347–352, 1978.

[10] G. Baum *et al.*, "A New Measurement of Deep Inelastic Electron-Proton Asymmetries," *Phys. Rev. Lett.* **51**, pp. 1135–1138, 1983.

[11] D. Kawall *et al.*, "Large Volume Threshold Čerenkov Counters," presented at this symposium.

[12] P. A. Souder, private communication.

[13] H. Fonvieille, private communication.

[14] G. T. Bartha *et al.*, "Design and Performance of the ASP Lead-Glass Calorimeter," *Nucl. Instr. Methods* **A275**, pp. 59–70, 1989.

[15] K. L. Brown, "A First- and Second-Order Matrix Theory for the Design of Beam Transport Systems and Charge Particle Spectrometers," SLAC Report–75, 1982.

[16] J. S. McCarthy and C. Y. Prescott, private communication.

[17] C. Y. Prescott, private communication.